HHS Public Access

Author manuscript

Nat Neurosci. Author manuscript; available in PMC 2014 January 01.

Published in final edited form as:

Nat Neurosci. 2013 July ; 16(7): 903–909. doi:10.1038/nn.3415.

Circuit level defects in the developing neocortex of fragile X mice

J. Tiago Gonçalves[1,*], **James E. Anstey**[1,Ŧ], **Peyman Golshani**, and **Carlos Portera-Cailliau**[1,2]

[1]Department of Neurology, David Geffen School of Medicine at UCLA, 710 Westwood Plaza, Los Angeles, CA 90095.

[2]Department of Neurobiology, David Geffen School of Medicine at UCLA, 710 Westwood Plaza, Los Angeles, CA 90095.

Abstract

Subtle alterations in how cortical network dynamics are modulated by different behavioral states could disrupt normal brain function and underlie symptoms of neuropsychiatric disorders, including fragile X syndrome (FXS). Using two-photon calcium imaging and electrophysiology we recorded spontaneous neuronal ensemble activity in mouse somatosensory cortex. Unanesthetized *Fmr1*$^{-/-}$ mice exhibited abnormally high synchrony of neocortical network activity, especially during the first two postnatal weeks. Neuronal firing rates were 3-fold higher in *Fmr1*$^{-/-}$ mice during whole-cell recordings manifesting Up/Down states (slow wave sleep, quiet wakefulness), likely due to a higher firing probability during Up states. Combined EEG/calcium imaging experiments confirmed that neurons in mutant mice have abnormally high firing and synchrony during sleep. We conclude that cortical networks in FXS are hyperexcitable in a brain state-dependent manner during a critical period for experience-dependent plasticity. These state-dependent network defects could explain the intellectual, sleep and sensory integration dysfunctions associated with FXS.

Keywords

2-photon; anesthesia; barrel cortex; calcium imaging; electrophysiology; fragile X syndrome; GABA; mGluR; network; patch clamp; sleep; slow cortical oscillation; two-photon; Up and Down states; wakefulness

Corresponding author: Carlos Portera-Cailliau, MD-PhD 710 Westwood Plaza, RNRC A-145 Los Angeles, CA 90095 cpcailliau@mednet.ucla.edu.

*Present address: The Salk Institute for Biological Studies, Laboratory of Genetics, 10010 North Torrey Pines Road, La Jolla, CA 92037

Ŧ Present address: Oregon Health & Science University School of Medicine, Portland, Oregon 97239

Author contributions:

JTG and CPC conceived the project and designed the experiments. JTG, JEA and PG conducted the experiments and analyzed the data. JTG and CPC prepared the figures and wrote the manuscript. CPC supervised the project.

Competing financial interests:

The authors declare no competing financial interests.

Introduction

Spontaneous activity in the cerebral cortex, the ongoing neuronal firing that occurs independently of external inputs, is thought to underlie attention, the expectation of a sensory stimulus, or other cognitive functions that are important for encoding information about our surrounding environment [1]. Because this activity is intrinsically generated in the cortex, internal brain states play a critical role in shaping sensory perception, learning and cognition [2]. In rodents, processing of sensory inputs from whiskers on the snout by neurons in barrel cortex is markedly different in quiet wakefulness compared to active whisking [3]. Thus, neuronal activity in neocortex can vary greatly depending on the state of vigilance of the animal, and this top-down modulation of network dynamics with different behavioral states is an essential part of normal brain function. For example, sleep replay of awake experience in the cortex is probably critical for memory consolidation [4]. Additionally, spontaneous activity during development is crucial for the shaping of neuronal networks [5], such that changes in activity patterns during critical periods for experience-dependent plasticity can lead to functional miswiring of cortical circuits [6]. Conceivably, this means that subtle defects in neuronal ensemble dynamics that alter spontaneous replay and learning, particularly at early stages of cortical development, could result in intellectual dysfunction or autism.

Autism spectrum disorders, which are characterized by impaired social interactions, disrupted communication and highly restricted or repetitive behaviors [7], are believed to be caused by developmental defects in brain connectivity[8]. Subtle anatomical and functional abnormalities have been reported at the level of synapses in various types of autism and mental impairment, including fragile X syndrome (FXS) [9]. In contrast, little is known about circuit-level alterations that could more easily account for the profound behavioral and intellectual deficits seen in affected individuals. For instance, hyperexcitability in cortical networks, as shown by several elegant studies in *Fmr1*$^{-/-}$ mice[10-13], may explain their hyperarousal, propensity to seizures and hypersensitivity to sensory stimuli[14]. Such hyperexcitability could be triggered by defects in how network activity emerges in the cortex during development[15] or how it is modulated by different behavioral brain states[16]. But despite the importance of neural microcircuits in sensory processing and cognition, these basic questions about network dynamics in FXS have not yet been thoroughly investigated, especially in vivo. In part, this is because the tools necessary to study how activity propagates within intact cortical circuits during development have only recently become available. Optical probing of neuronal activity with two-photon calcium imaging is particularly well-suited to study network function in large ensembles of neurons in the living brain [17].

Here, our goal was to record neuronal ensemble dynamics within intact cortical circuits in the *Fmr1*$^{-/-}$ mouse model of FXS to bridge the gap that exists between the known synaptic defects on one hand, and the well-described cognitive-behavioral abnormalities on the other. We focused on early postnatal development because FXS has a childhood onset and many of the symptoms (seizures, sleep disturbances) are more prominent at young ages. At around postnatal day (P) 12 in wild-type (WT) mice, the neocortex undergoes an abrupt desynchronization of spontaneous network activity [15,18]. This major network transition into

sparse neuronal firing is a critical step in brain maturation that allows for more efficient neural coding. Here we tested the hypothesis that *Fmr1*$^{-/-}$ mice exhibit defects in the desynchronization of cortical network activity and in state-dependent modulation of neuronal firing. We used in vivo calcium imaging of population activity, patch clamp recordings and electroencephalography (EEG) in barrel cortex of WT and *Fmr1*$^{-/-}$ mice. We asked the following questions: 1. Do *Fmr1*$^{-/-}$ mice undergo a normal desynchronization of network activity? 2. Is there evidence of hyperexcitability in vivo? 3. Do mutant mice exhibit defects in network synchrony or neuronal firing during specific brain states (i.e., slow wave sleep vs. wakefulness)?

Results

Cortical network synchrony is high in *Fmr1*$^{-/-}$ mice

The developmental decorrelation of neuronal ensemble activity[15,18] is a fundamental step in cortical maturation because it enhances the efficiency of sparse population coding of natural stimuli. Therefore, we hypothesized that perturbations in network desynchronization could lead to network dysrhythmias that may underlie a number of disorders, including autism[15]. To test this prediction, we examined the spontaneous activity of large ensembles layer (L) 2/3 neurons in barrel cortex with in vivo two-photon calcium imaging, using the fluorescent indicator Oregon Green BAPTA-1 in head-fixed mice at different postnatal ages, before and after the 2nd postnatal week (**Fig. 1a, b**). Our calcium imaging experiments confirmed several findings of our earlier study. First, cortical neurons in unanesthetized WT mice show a higher degree of synchrony in the transient elevations of intracellular calcium at P9-11 than at the later time points of P14-16 or P30-40 (**Fig. 1c**). Second, cell pairs located within 100 μm of one another displayed the largest differences in pair-wise correlation coefficients between P9-11 (n = 12 mice) and P14-16 (n = 9 mice), compared to cells farther apart (mean difference 0.223, $p<0.0001$ for cells <100 μm apart, 0.159, $p<0.0001$ for cells 100-200 μm apart and 0.067, $p=0.0598$ for cells >200 μm apart; two-way ANOVA with Bonferroni corrected p values; **Fig. 1d**). When we quantified pairwise correlation coefficients for cells within 100 μm, we found a statistically significant age-dependent decrease in network synchrony for both WT and *Fmr1*$^{-/-}$ mice (two-way unequal variance ANOVA, $p<0.01$ for both genotypes; n = 12, 9, 8 WT mice at P9-11, P14-16, and P30-40, respectively and n = 9, 10, 8 *Fmr1*$^{-/-}$ mice at the same ages, respectively; **Fig. 1e**). In addition, when we compared the two genotypes, we found significantly higher correlation coefficients for cell pairs in *Fmr1*$^{-/-}$ mice when pooling data for all ages (average corr. coefficient 0.230 ± 0.008 for WT vs. 0.265 ± 0.009 for *Fmr1*$^{-/-}$, $p = 0.0057$, two-way unequal variance ANOVA). Similar results were found when we calculated correlation coefficients using the Pearson method (average corr. coefficient 0.164 ± 0.009 for WT vs. 0.196 ± 0.010 for *Fmr1*$^{-/-}$, $p = 0.026$, two-way unequal-variance ANOVA; **Suppl. Fig. 1**). The difference in correlation coefficients was most pronounced at P14-16 (0.172 ± 0.012 for WT vs. 0.210 ± 0.011 for *Fmr1*$^{-/-}$, $p=0.032$, t-test; average age: 14.7 and 15.1 days for WT and *Fmr1*$^{-/-}$, respectively; **Fig. 1e, f**). By P30-40, this difference in correlation coefficients in mice of both genotypes had decreased (0.144 ± 0.008 vs. 0.123 ± 0.008 for *Fmr1*$^{-/-}$ and WT respectively, $p = 0.075$, t-test), suggesting that changes in network synchrony in the mutant mice might potentially normalize with age. This is reminiscent of other studies reporting transient defects in the

maturation of neocortical circuits in *Fmr1*$^{-/-}$ mice, such as a delay in the stabilization of dendritic spines or in the window for plasticity during critical periods of barrel cortex development [19-21]. Because the biggest differences in correlation coefficients between WT and *Fmr1*$^{-/-}$ mice were observed at P14-16 and this age corresponds to a critical period of development for barrel cortex[22], we focused on this age group for subsequent experiments.

Next, we investigated the network causes of the higher synchrony in mutant mice and considered several possibilities, including a higher frequency of periodic bursts of synchronous firing (a.k.a., peaks of synchrony [23]), a greater proportion of neurons participating in those peaks of synchrony, or higher firing rates overall. First, we estimated the occurrence of peaks of synchrony, defined as network events with a significantly higher proportion of neurons participating than would be expected by chance alone (see Methods; **Fig. 2a**). The frequency of peaks of synchrony was slightly higher in *Fmr1*$^{-/-}$ mice at P14-16, but the difference was not significant (0.060 ± 0.007 vs. 0.053 ± 0.006 peaks per s for *Fmr1*$^{-/-}$ and WT, n = 9 and 10 mice, respectively; p=0.45; t-test; **Fig. 2b**). However the proportion of neurons that participated in peaks of synchrony was significantly higher in *Fmr1*$^{-/-}$ mice than in WT mice at P14-16 (0.380 ± 0.023 vs. 0.300 ± 0.017 for *Fmr1*$^{-/-}$ and WT respectively; p = 0.023; t-test; **Fig. 2c**). Finally, we calculated neuronal firing rates, as extrapolated from calcium imaging data by temporal deconvolution (see Methods), but could not detect differences between genotypes at any age using this method (not shown). We conclude that the higher correlation coefficients in *Fmr1*$^{-/-}$ mice at P14-16 are explained, at least in part, by a higher than normal proportion of neurons participating in peaks of synchrony.

High firing rates during Up/Down states *Fmr1*$^{-/-}$ mice

In order to assess whether *Fmr1*$^{-/-}$ mice had higher firing rates than WT mice as an explanation for the higher correlation coefficients we turned to in vivo electrophysiology (**Fig. 3a**). We carried out whole-cell recordings in L2/3 neurons in head-fixed unanesthetized WT and *Fmr1*$^{-/-}$ mice at P14-16 (n = 7 and 12, average age: 15.3 and 15.2 days, respectively; **Fig. 3b**). First, we established that action potential kinetics were indistinguishable between WT and *Fmr1*$^{-/-}$ mice (**Suppl. Fig. 2**). Our recordings demonstrated that mice exhibited different brain states, as some cells transitioned between two types of activity (**Fig. 3b**): fast oscillatory activity (FOA) typical of wakefulness (or REM sleep), and Up/Down states typical of sleep or quiet wakefulness [24,25]. In order to sort recording segments manifesting FOA from those with clear Up/Down states, we started by calculating frequency histograms for every sampled membrane voltage[26]. Since Up/Down state segments are characterized by a preference for two resting membrane potentials we were able to distinguish them from FOA activity with a semi-automated algorithm that used iterative fits to find segments with bimodal membrane voltage distributions (see Methods; **Fig. 3c, d**). We discovered that L2/3 neurons in *Fmr1*$^{-/-}$ mice had 3-fold higher firing rates than WT mice during Up-Down states (0.40 ± 0.05 Hz, n = 6 recordings from 6 cells in 4 mice vs. 0.13 ± 0.04 Hz, n = 5 recordings from 5 cells in 5 mice; Bonferroni corrected p = 0.040, 2-way ANOVA; **Fig. 3e**). There was a trend toward higher firing rates in WT mice during FOA segments compared to Up/Down states, but this was not significant (0.133 ± 0.036 Hz, n = 5 recordings from 5 cells in 5 mice vs. 0.290 ± 0.158 Hz, n = 4 recordings

from 4 cells in 4 mice, Bonferroni corrected p = 0.41, 2-way ANOVA), which is in agreement with previous studies [16,25]. There was also an opposite trend for *Fmr1*$^{-/-}$ mice, which showed a tendency toward higher firing rates during Up/Down states compared to FOA, and together this probably explained the significantly higher firing rates in *Fmr1*$^{-/-}$ mice compared to WT mice during recordings with Up/Down states. In addition, we found that recorded neurons in *Fmr1*$^{-/-}$ mice spent approximately the same amount of time as WT mice in the FOA brain state (56% and 52%, respectively; **Fig. 3f**), which suggests that the differences in firing rates (or correlation coefficients) were not due to differences in the overall state of vigilance of mice from either genotype.

It has recently been shown that L4 excitatory neurons from *Fmr1*$^{-/-}$ mice have longer thalamically evoked Up states [12] and longer spontaneously occurring Up states than WT mice [27]. However, in our vivo whole-cell recordings of L2/3 neurons in unanesthetized mice at P14-16 we found no significant differences between WT and *Fmr1*$^{-/-}$ mice in the duration of Up states (1.30 ± 0.06 s, n = 5 cells vs.1.29 ± 0.14 s, n = 6 cells, respectively; p = 0.92, t-test; **Fig. 4a-c**), in the frequency of Up states (0.38 ± 0.03 Hz vs. 0.36 ± 0.02 Hz; p = 0.64, t-test; **Fig. 4d**), or in the Up-Down step (7.05 ± 0.86 mV vs. 8.85 ± 0.99 mV; p = 0.21, t-test; **Fig. 4e**). Next, we investigated whether the higher firing rates in *Fmr1*$^{-/-}$ mice during Up/Down states were caused by the mutant animals having on average more active Up states (those with 1 or more spikes) and fewer silent Up states (those with no spikes), or by *Fmr1*$^{-/-}$ mice firing more action potentials per active Up state. Although we found a strong trend toward a higher number of action potentials per active Up state in *Fmr1*$^{-/-}$ mice, this difference was not significant (2.57 ± 0.38, n = 6 cells vs. 1.67± 0.18, n = 5 cells spikes in *Fmr1*$^{-/-}$ and WT mice, respectively; p = 0.079, t-test; **Fig. 4f**). In contrast, the firing probability during any given Up state was 2-fold higher in the mutants (0.45 ± 0.05, n = 6 cells vs. 0.21 ± 0.05, n = 5 cells; p = 0.009, t-test; **Fig. 4g**). Thus, the fact that *Fmr1*$^{-/-}$ mice have fewer silent Up states explains their higher firing rates during Up/Down states (**Fig. 3e**). Overall, our in vivo electrophysiology data suggests that the mutant mice have unusually high firing rates at times of quiet restfulness (or sleep), which could interfere with coordinated replay of ensemble-level patterns of activity and the normal process of memory consolidation [4]. This elevated firing rate, owing to a higher likelihood of having active Up states, also likely explains the higher correlation coefficients we observed with calcium imaging.

Brain state-dependent defects in activity modulation

To further investigate the relationship between brain states and cortical network activity, we conducted experiments with simultaneous calcium imaging and EEG recordings in a subset of the WT and *Fmr1*$^{-/-}$ mice analyzed in Fig. 1 (**Fig. 5a**). We computed the ratio between the EEG power in low (0.5-4.0 Hz) and high (20-60 Hz) frequency ranges (L/H power; **Fig. 5b**), which has been previously utilized as a measure of the overall behavioral state of the animal [28]. In WT mice at P14-16 (n = 5 mice, average age 14.6 days), we found that firing rates (extrapolated from calcium traces) did not vary significantly between recordings exhibiting high L/H power (expected during sleep) or low L/H power (expected during wakefulness) (r^2 = 0.046, n = 13 recordings, p = 0.481, F-test; **Fig. 5c**). This is analogous to our results with whole-cell recordings that showed no modulation of neuronal firing between

different brain states in WT mice (**Fig. 3e**). In contrast, the firing of L2/3 neurons in *Fmr1*$^{-/-}$ mice at P14-16 (n = 5 mice, average age 15.0 days) was significantly correlated with L/H power (r^2 = 0.676, n = 10 recordings p = 0.004, F-test; **Fig. 5c**). This increase in firing rates when *Fmr1*$^{-/-}$ animals manifest the EEG signature of slow wave sleep was reminiscent of our results with in vivo electrophysiology (i.e., higher firing rates during Up/Down states; **Fig. 3e**). The strong correlation between neuronal firing and L/H power in the EEG was still present at P30-40 in *Fmr1*$^{-/-}$ mice, but not WT mice (r^2 = 0.73, n = 10 recordings from 4 mice, p = 0.002 for *Fmr1*$^{-/-}$ vs. r^2 = 0.027, n = 10 WT recordings from 4 mice, p = 0.65 for WT, F-test; not shown), which implies that some of the network alterations in *Fmr1*$^{-/-}$ mice persist in adulthood. Pair-wise correlation coefficients (as determined from calcium traces; 100 μm distance between pairs) showed a nearly-significant trend toward higher synchrony with higher L/H power in *Fmr1*$^{-/-}$ mice at P14-16, but not in WT mice (r^2 = 0.347, n = 10 recordings, with p=0.073 vs. r^2 = 0.027, n = 13 recordings with p = 0.649, F-test, for *Fmr1*$^{-/-}$ and WT, respectively; **Fig. 5d**). However, when we examined only EEG epochs with L/H power > 200, which others have used an arbitrary cut off that represents slow-wave sleep [28], we found that *Fmr1*$^{-/-}$ mice had higher firing rates (0.27 ± 0.017 Hz, n = 5 *Fmr1*$^{-/-}$ recordings vs. 0.22 ± 0.0096 Hz, n = 6 WT recordings, p=0.023, t-test; **Fig. 5e**) and higher correlation coefficients than WT mice (0.25 ± 0.014, n = 5 *Fmr1*$^{-/-}$ recordings, 0.20 ± 0.015, n = 6 WT recordings, p=0.039, t-test; **Fig. 5f**; same results with Pearson method, **Suppl. Fig. 3**).

To evaluate the effect of firing rate on correlation coefficients, we plotted these two variables and found that, whereas in WT mice they are not correlated (r^2=0.005, n = 13 recordings, p=0.46, F-test), in *Fmr1*$^{-/-}$ mice they were highly correlated (r^2=0.65, n = 10 recordings, p=0.0027; F-test, **Suppl. Fig. 4a**). In particular, it was the mutant mice exhibiting L/H power > 200 with higher firing rates that drove up the correlation coefficients. Thus, we conclude that the higher synchrony of *Fmr1*$^{-/-}$ mice, at least P14-16, was due to higher firing rates occurring at times of sleep or quiet wakefulness (**Figs. 3e, 5e, Suppl. Fig. 4b**), in addition to the higher proportion of neurons participating in peaks of synchrony (**Fig. 2c**). During these short recordings (< 2 h, in the dark), the average L/H power was similar between WT and *Fmr1*$^{-/-}$ mice (176.1 ± 29.55, n = 10 recordings, 180.2 ± 30.58, n = 13 recordings, respectively, p = 0.92, t-test; **Fig. 5g**), suggesting that they spend similar amounts of time in sleep and wakefulness and that the differences in neuronal activity between genotypes were not caused by mice exhibiting different brain states.

One potential concern is that, even though two-photon calcium imaging at 3.9 Hz is excellent at detecting bursts of 2 or more action potentials, it is less reliable for detecting isolated single spikes [15], and this could affect these results. Still, when we performed calcium imaging at 15.6 Hz (which provides better spike detection) we again found that firing rates increased significantly with higher L/H power in *Fmr1*$^{-/-}$ mice, but not WT mice at P14-16 (r^2 = 0.38, n = 12 recordings from 4 mice, p = 0.032 in *Fmr1*$^{-/-}$ vs. r^2 = 0.11, n = 10 recordings from 5 mice, p = 0.35 in WT, F-test; not shown). We also obtained similar results when we used Power Δ/ Power θ [29] (instead of L/H power) as a measure of different brain states (not shown).

Network activity is unchanged by anesthesia in mutant mice

Because cortical neurons in *Fmr1*$^{-/-}$ animals exhibited higher than normal firing rates during Up/Down states and during high L/H EEG epochs (both consistent with a sleep-like state or quiet wakefulness), we wondered how the mutant mice would respond to anesthesia, which induces a single brain state characterized by the slow cortical oscillation and Up/Down states [24] and increases pair-wise correlations in WT mice [15]. Using in vivo calcium imaging, we examined ensemble network activity in L2/3 neurons of mice anesthetized with isoflurane (1-2%) at P14-16. We confirmed that pair-wise correlation coefficients for cells within 100 μm were significantly higher in isoflurane-anesthetized WT mice than in unanesthetized WT mice (0.24 ± 0.02 vs. 0.17 ± 0.01, n = 9 and 9 mice, respectively; p=0.0045, t-test; **Fig. 6a, c**). In contrast, correlation coefficients in *Fmr1*$^{-/-}$ mice were unchanged by isoflurane anesthesia (0.21 ± 0.01 vs. 0.18 ± 0.01, n=10 and 10 mice, respectively, p=0.14, t-test; **Fig. 6 b, d**).

Similarly, isoflurane had a significant effect on extrapolated firing rates of L2/3 neurons in WT mice (0.30 ± 0.03 vs. 0.21 ± 0.02 Hz for unanesthetized and isoflurane, respectively, p=0.0084, t-test), but did not change neuronal firing in *Fmr1*$^{-/-}$ mice (0.29± 0.03 vs. 0.27 ± 0.02 Hz for unanesthetized and isoflurane, respectively, p=0.62, t-test). Because the effects of isoflurane are thought to be partially mediated by facilitation of inhibitory $GABA_A$ receptors in the brain [30,31], our anesthesia results suggest that the elevated network synchrony and higher firing rates in *Fmr1*$^{-/-}$ mice (both consistent with network hyperexcitability) could be due to defects in inhibition in the mutant animals.

Discussion

Over the last two decades, various defects at the level of dendritic spines and alterations in synaptic plasticity have been reported in *Fmr1*$^{-/-}$ mice [9,32]. At the same time, our understanding of the molecular signaling cascades regulated by the fragile X mental retardation protein (FMRP) has increased rapidly [33]. Despite these advances, we still know very little about the circuit level abnormalities in FXS that underlie the known cognitive and behavioral deficits of affected individuals. One of the main motivations for the present study was to fill this knowledge gap by using in vivo calcium imaging and electrophysiology to uncover new cortical network phenotypes in fragile X mice. Our main findings can be summarized as follows: 1. *Fmr1*$^{-/-}$ mice exhibit abnormally high synchrony in the firing of cortical neurons, especially during the first 2 postnatal weeks; 2. Firing rates of cortical L2/3 pyramidal neurons are abnormally elevated in mutant mice during Up/Down states, owing to a higher firing probability during Up states; 3. Network synchrony in *Fmr1*$^{-/-}$ mice is not modulated by anesthesia the way it is in WT mice.

A sharp decrease in the correlated firing of cortical neurons (occurring in the second postnatal week in mice) is an essential step in the development of the neocortex [15,18]. This desynchronization of spontaneous network activity gives rise to sparse coding, a general feature of information processing in mature sensory cortices that is computationally efficient because it increases memory storage capacity, simplifies the representation of complex data, and saves energy [34]. In addition, intrinsically generated activity in the cerebral cortex can influence several cognitive functions that are critical for normal computations [2]. Therefore,

the fact that neurons in somatosensory cortex of *Fmr1*$^{-/-}$ mice exhibit elevated pairwise correlation coefficients is expected to have profound consequences on the brain's ability to decipher sensory signals and thereby negatively impact animal behavior. Importantly, the higher synchrony in neuronal firing of early postnatal *Fmr1*$^{-/-}$ mice might explain the propensity of children with FXS (and the mutant mice) for seizures [35]. Thus, our study identifies the underpinnings of network dysfunction in a model of autism and intellectual impairment. Given the widespread expression of FMRP, one imagines that this represents a generalized cortical phenomenon. Why was such high network synchrony not seen in the EEG? The reason may be that EEG recordings reflect the activity of a very large population of neurons and therefore may not be sensitive enough to detect a relatively subtle (~20% increase in synchrony), particularly if changes are restricted to one cortical layer. Interestingly, there is one recent report of reduced alpha and exaggerated theta power during resting-state EEG in individuals with FXS [36].

What might explain the high synchrony of cortical network activity in *Fmr1*$^{-/-}$ mice? First, defects in the maturation of the cerebral cortex have been reported in these mice from an anatomical point of view, which could contribute to neuronal signaling problems. For example, dendritic spines in neocortical neurons are not only immature morphologically [37], but also abnormally unstable during the 2nd postnatal week [19]. Axonal arbors of the L4 → L3 projection are also spatially diffuse in the mutant mice at 2 weeks of age [20], suggesting that they might fail to develop properly. Notably, a defect of hyper-connectivity has been uncovered in L5 pyramidal neurons of *Fmr1*$^{-/-}$ mice, but again only transiently during early postnatal development[13]. Both of these studies are consistent with our findings because they point to potentially transient problems in the maturation of brain circuits during a critical period for experience-dependent plasticity in neocortex and because the nature of the changes (hyper-connectivity) could explain the increases in neuronal synchrony. Second, the known deficiencies in $GABA_A$ signaling in *Fmr1*$^{-/-}$ mice [38] could explain the higher firing rates in neocortical neurons that we describe. Third, L4 excitatory neurons in 4 week-old *Fmr1*$^{-/-}$ mice have a higher than normal input resistance and are intrinsically more excitable [12], which could also explain the increased firing and synchrony. It is worth noting that the functional and structural alterations in cortical circuits that we and others have described in the mutant mice all occur during roughly the same critical period between the 2nd and 3rd postnatal weeks. Hence, our data provide further support to the theory that autism is a disorder of critical periods taking place during the development of sensory cortices [39,40].

Our findings that the activity of cortical neurons in *Fmr1*$^{-/-}$ mice is not modulated by anesthetics and that firing rates are abnormally high during brain states corresponding to sleep, raise the possibility that the mutant mice might experience an elevated state of vigilance, or hyperarousal during sleep. This could explain some of known alterations in circadian rhythms in this disorder, such as the fact that individuals with FXS suffer from sleep disturbances, especially frequent night awakenings [41]. Indeed, *FMR1* and its vertebrate paralog *FXR2* are required for rhythmic circadian behavior [42], and the Drosophila fragile X mental retardation gene is known to regulate sleep need [43]. The exact function of sleep has not been fully elucidated, but experimental evidence suggests it plays a role in memory

consolidation [4]. The slow cortical oscillation (<1 Hz), during which neurons exhibit membrane potential fluctuations known as Up/Down states, is the characteristic feature of the EEG during non-REM sleep and quiet wakefulness [44]. Alterations in neuronal activity during sleep would likely have dire consequences on the computational abilities of the cerebral cortex. The fact that we uncovered a specific problem of *Fmr1*$^{-/-}$ mice in modulating neuronal firing rates during Up/Down states suggests that, even if the neocortex of mutant mice can adequately perform neural computations during wakefulness, it may not be able to encode information during slow-wave sleep.

As an aside, it has been reported that *Fmr1*$^{-/-}$ mice have prolonged Up States both in acute brain slices and in anesthetized mice in vivo [27]. Intriguingly, we did not detect differences in the length of Up states in *Fmr1*$^{-/-}$ mice. Perhaps differences in how the slow oscillation was measured (in vivo whole-cell recordings in unanesthetized mice vs. whole-cell recordings in slices or extracellular recordings under urethane), the cell type recorded (L2/3 vs. L4 and L5), or the age of the animal, can explain these results. For instance, it is conceivable that prolonged Up states in L4 (an initial form of hyper-excitability) lead to higher firing rates in L2/3 neurons (a secondary form of hyper-excitability) but without prolonging Up states. Thus, our observations of higher firing rates during Up states in vivo extend those previous results in providing evidence of increased cortical excitability in *Fmr1*$^{-/-}$ mice[12], and support the theory of impaired inhibition in FXS. Our findings are novel in that they reveal a brain-state dependent change in firing of pyramidal neurons that could not previously be appreciated in brain slices or in anesthetized animals. This result is interesting not only in the context of FXS research, but also because it constitutes the first description of a network defect that manifests itself only under a specific brain state.

Our data pointing to a problem of hyperexcitability in *Fmr1*$^{-/-}$ fit nicely with the idea that the balance of excitation and inhibition is dysregulated in FXS. Children with FXS experience hypersensitivity to sensory stimuli [14] and many have seizures [45], so our data provide a possible network basis for these symptoms. Importantly, the notion of hyperexcitable networks may apply to autism in general[46,47]. Therefore, other forms of autism or mental impairment may also exhibit alterations in the network synchronization that we have identified in FXS, raising the possibility that identifying a treatment strategy to correct these defects may be applicable to a variety of neurodevelopmental disorders. One such strategy is to modulate GABAergic inhibition. Our data are also consistent with impairments in inhibition in the neocortex of fragile X mice, as evidenced by the elevated firing rates and insensitivity to anesthesia. The reduced expression of certain GABA receptor subunits in *Fmr1*$^{-/-}$ mice[11,48] could explain why anesthesia, which normally enhances inhibition and entrains neurons to fire together (leading to higher correlation coefficients in WT mice) had no effect on network synchrony in the mutants. Of note, somatostatin-expressing and parvalbumin-expressing interneurons in L2/3 are more active during periods of quiet wakefulness (and sleep) and the former in particular suppress their firing during whisker stimulation [49]. Therefore, the lower in parvalbumin interneuron density in *Fmr1*$^{-/-}$ mice [50] (or yet to be identified reductions in somatostatin neuron density) could explain the increased firing rates we observed in the mutant mice during Up/Down states. Future experiments will need to further elucidate the specific defects in inhibition in

FXS and test whether GABAergic drugs could be of therapeutic value in this devastating disorder.

Online Methods

All materials were purchased from Sigma-Aldrich (St. Louis, MO) unless otherwise stated.

Experimental animals

All experiments were conducted according the National Institutes of Health guidelines for animal research, under an animal protocol (ARC#2007-035) approved by the Chancellor's Animal Research Committee (ARC) and the Office for the Protection of Research Subjects (OPRS) at the University of California, Los Angeles. Male and female C57Bl/6 WT and *Fmr1*$^{-/-}$ mice[51] were used in all experiments at ages P9-40. Mice were housed in a vivarium under a 12h light/dark cycle; all experiments were acute (i.e., mice were not returned to the vivarium after surgery) and were done during the light phase of the cycle. Animals were weaned at P21 and group housed (up to 4 animals per cage); younger animals (<P21) were housed with a lactating dam, and occasionally with another adult female mouse.

Cranial window surgery and calcium dye injection

Mice were anesthetized with isoflurane (1.5% via a nose cone) and placed in a stereotaxic frame. A ~2 mm diameter craniotomy was performed over the right barrel cortex and partially covered with a glass coverslip, as previously described[15,52]. A well was made from dental cement around the cranial window to hold a meniscus of cortex buffer [in mM: NaCl 125, KCl 5, glucose 10, HEPES 10, $CaCl_2$ 2, $MgSO_4$ 2] for the water dipping objective. A small titanium bar was also attached to the skull with dental cement to secure the animal to the microscope stage. Mice were then transferred to the two-photon microscope and head-fixed to the stage while under isoflurane anesthesia. For dye injections, we prepared 1 mM Oregon-Green BAPTA-1 AM (OGB) (Invitrogen, Carlsbad, CA) in DMSO/Pluronic and 100 μM Sulforhodamine-101 (SR) to visualize astrocytes as previously described [52]. Glass microelectrode pipettes (2-4 MΩ) were pulled (Sutter Instruments P-97, Novato, CA) and filled with the OGB solution. The OGB solution was pressure injected at 10 PSI for 1 min (Picospritzer, General Valve, Brookshire, MA), at a depth of 200 μm below the dura. Typically 2-4 injections, spaced 200-300 μm apart, were needed to label an area measuring 500 by 500 μm in the *xy* plane.

In vivo two-photon calcium imaging in head-restrained mice

For calcium imaging we used a custom-built two-photon microscope using a Ti-Sapphire laser (Chameleon XR, Coherent, Santa Clara, CA) tuned to 800nm. For experiments in anesthetized animals, we used light isoflurane anesthesia (< 1.0 % for ages > P14 and 1-1.5 % for P9-11). Mice were kept at 37°C using a temperature control device with a rectal probe (Harvard Apparatus, Boston, MA). For experiments with unanesthetized animals, imaging began within 30-60 min of stopping the flow of isoflurane after the last OGB injection. The respiration rate was monitored frequently during imaging sessions in anesthetized mice and kept at 90-100 breaths/minute. Calcium imaging could be performed over 1-2 hours periods, during which the head restrained mice were allowed to whisk, groom, sleep or rest quietly.

Mice did not exhibit signs of pain or distress during the in vivo imaging (or electrophysiological recordings, described below). Images were acquired using ScanImage software [53] written in MATLAB (MathWorks, Natick, MA). Laser power was maintained well below 70 mW at the sample. Whole field images were collected using a 20X 0.95 NA objective (Olympus, Center Valley, PA) at an acquisition speed of 3.9 Hz (512 × 128 pixels) or 15.6 Hz (512 × 32 pixels).

Data analysis for calcium imaging

Calcium imaging data were analyzed using custom routines in MATLAB, as previously described [15]. Several 3-min calcium movies were concatenated and brief segments of motion artifact (<10 s over a 3 min movie) were removed as needed. To correct for slight *x-y* drift, movies were then aligned using cross-correlation-based, sub-pixel image registration routine[54]. Contours around OGB labeled cells were automatically detected and drawn in the average intensity xy*t* stack projection image of the entire movie using custom algorithms. Neuronal, and neuropil signals were analyzed separately and astrocytic signals were excluded from analysis. The average ΔF/F signal of each cell body was calculated at each time point. Each ΔF/F trace was low pass filtered and deconvolved, as previously described[15,55]. We extrapolated firing rates from calcium traces (based on previous control experiments using simultaneous cell-attached recordings and calcium imaging) and pair-wise continuous-trace cross-correlations as previously described [15].

To calculate frequency, duration, and estimated firing rates during network events (peaks of synchrony) we first marked the temporal boundaries of network events. This was performed by constructing activity histograms that plotted the percent of cells that were active for each frame of each movie. The threshold for detection of a network event was set by repeatedly shuffling each deconvolved somatic calcium trace 100 times, while maintaining the average firing rate for each cell constant. A surrogate activity histogram was constructed from each reshuffled trial. The threshold was calculated by first finding the peak percentage of cells active in each reshuffled trial, and then sorting these values to find the 95th percentile, which was set as the threshold for significance (p=0.05). The time point when the percent of cells active exceeded this threshold was set as the start of an event and the time point when the percentage of cells active fell below this level was set as the end of the event. Full widths at half-maximum of calcium transients were calculated in MATLAB using the iPeak software package (http://terpconnect.umd.edu/~toh/spectrum), and no differences were found between WT and *Fmr1*$^{-/-}$ mice (not shown).

In vivo patch-clamp recordings in unanesthetized mice

A silver-chloride ground wire insulated with Teflon (except at the tip) was passed through a burr hole over the cerebellum and fixed with dental cement at the time of the cranial window surgery. Mice were allowed to awaken from isoflurane anesthesia on the microscope stage and kept at 37 °C. Patch clamp recordings of L2/3 pyramidal neurons were performed in vivo in whole-cell configuration through a cranial window (Multiclamp, Molecular Devices, Sunnyvale, CA). For current clamp recordings we used borosilicate microelectrodes (4-6 MΩ) containing potassium gluconate based-solution (in mM): 105 K-gluconate, 30 KCl, 10 HEPES, 10 phosphocreatine, 4 ATP-Mg, 0.3 GTP (adjusted to pH 7.3 with KOH). Series

resistance was typically between 30 and 90 MΩ. The holding potential in voltage clamp recordings was corrected for series resistance error. Data was digitized at 20 kHz (Digidata, Molecular Devices, Sunnyvale, CA) and analyzed in MATLAB using custom routines. Action potentials were detected using a simple threshold set to -20 mV. We did not analyze data from 1 cell with a firing rate <1 spike per min and another cell (presumably an interneuron) with a firing rate >2 standard deviations higher than the average of all other cells.

For Up/Down state detection, we plotted frequency histograms for every sampled membrane voltage[26]. Recordings were then segmented into 30 s epochs and activity in each epoch was classified as either “Up/Down state” or “fast oscillatory activity” (FOA) categories by successively fitting a two-Gaussian mixture to the voltage distribution using an Expectation Maximization algorithm (MATLAB). Segments in which the average of 20 fits converged with a mode mix fraction in the range of 25/75 to 45/55 and mode separation was larger than 5 mV were classed as Up/Down segments. All other segments were classed as FOA segments. For Up vs. Down state detection, traces were low-pass filtered at 3 Hz and the mean voltage calculated for every minute of recording. Up and Down state thresholds were defined as the mean voltage plus or minus half the standard deviation of voltages, respectively. An Up-state was detected whenever the membrane potential crossed the Up state threshold and the mean voltage remained above that threshold for at least 1s. A Down state was detected whenever the membrane potential fell below the Down state threshold and the mean voltage remained below that threshold for at least 0.85 s. These parameters were empirically found to detect Up and Down states accurately (**Fig.3e, f**).

Electroencephalographic (EEG) recordings

During the cranial window surgery for calcium imaging, a custom-made bipolar tungsten electrode (0.002” tungsten wire, California Fine Wire, Grover Beach, CA) was implanted in an area immediately adjacent to the cranial window in the right barrel cortex (**Fig. 5a**). The electrode was lowered into the brain to a depth of 750 μm below the dura. A surface screw-type electrode was implanted at the equivalent location in the left hemisphere. Two ground electrodes were placed over the cerebellum. The electrodes, connecting wires and pins were held in place with dental cement. EEG data from 3-min recordings with simultaneous Ca2+ imaging were filtered (0.1-5000 Hz, 60 Hz notch filter), amplified (Model 1700, A-M Systems, Sequim, WA) and digitized (Digidata) at 10 kHz. Power spectra of EEG traces were calculated in MATLAB using the Chronux software package (http://chronux.org; [56]). In a subset of experiments, video recordings of the mice confirmed that when EEG traces exhibited high-frequency activity (i.e., low L/H power ratio) the animals were actively grooming or whisking, so we conclude that those recordings were unlikely to represent the brain state of rapid eye movement sleep.

Statistical Analyses

Threshold for significance (α) was set at 0.05. As tests of statistical significance we used unpaired two-tailed Student's t-tests, F-tests or ANOVA. To test for differences in correlation coefficients between WT and *Fmr1*$^{-/-}$ mice at different ages we used an unequal-variance, 2×3 fixed-effects ANOVA model, since variances were not constant across

different age groups. The Satterthwaite correction was used to compute error degrees of freedom under this model. P-values for post-hoc tests involving multiple comparisons were adjusted using the Bonferroni method. Variances and normality were analyzed when appropriate, in order to ensure that a suitable statistical test was chosen. In all figures, the error bars indicate the standard error of the mean, * indicates $p<0.05$, and ** indicates $p<0.01$. No randomization method was used to assign animals to the experimental groups and in some cases the experimenters were aware of the genotype of the animals. Regarding Up state duration, it is conceivable that we could have failed to detect a small (<22%) increase in Up state duration in *Fmr1*$^{-/-}$ mice given our confidence interval. Similarly, given the variance of the data on firing rates in Fig. 3, we could have missed subtle changes in firing rate of WT neurons between different brain states.

Supplementary Material

Refer to Web version on PubMed Central for supplementary material.

Acknowledgments

We thank Drs. Dean Buonomano, Carolyn Houser, Istvan Mody and Ricardo Mostany, as well as Mr. Daniel Cantu for helpful discussions and/or valuable comments on the manuscript. We also thank Drs. Anatol Bragin and Mark Blumberg for help with EEG recordings and interpretation, Dr. Jeffrey Gornbein and Ms. Daniela Markovich for help with statistical analyses, and Dr. William Greenough for providing the *Fmr1*$^{-/-}$ mice. This work was supported by grants from the NIH (NICHD R01HD054453 and NINDS RC1NS068093), FRAXA and the Dana Foundation.

Abbreviations

EEG	electroencephalography
FOA	fast oscillatory activity
FMRP	fragile X mental retardation protein
FXS	fragile X syndrome
GABA	gamma-amino butyric acid
L	layer
OGB-1	Oregon Green BAPTA-1
P	postnatal day
WT	wild-type

References

1. Arieli A, Sterkin A, Grinvald A, Aertsen A. Dynamics of ongoing activity: explanation of the large variability in evoked cortical responses. Science. 1996; 273:1868–1871. [PubMed: 8791593]
2. Gilbert CD, Sigman M. Brain states: top-down influences in sensory processing. Neuron. 2007; 54:677–696. [PubMed: 17553419]
3. Crochet S, Petersen CC. Correlating whisker behavior with membrane potential in barrel cortex of awake mice. Nat. Neurosci. 2006; 9:608–610. [PubMed: 16617340]

4. Ji D, Wilson MA. Coordinated memory replay in the visual cortex and hippocampus during sleep. Nat. Neurosci. 2007; 10:100–107. [PubMed: 17173043]
5. Katz LC, Shatz CJ. Synaptic activity and the construction of cortical circuits. Science. 1996; 274:1133–1138. [PubMed: 8895456]
6. Hensch TK. Critical period plasticity in local cortical circuits. Nat. Rev. Neurosci. 2005; 6:877–888. [PubMed: 16261181]
7. Rapin I, Katzman R. Neurobiology of autism. Ann. Neurol. 1998; 43:7–14. [PubMed: 9450763]
8. Geschwind DH, Levitt P. Autism spectrum disorders: developmental disconnection syndromes. Curr. Opin. Neurobiol. 2007; 17:103–111. [PubMed: 17275283]
9. Portera-Cailliau C. Which Comes First in Fragile X Syndrome, Dendritic Spine Dysgenesis or Defects in Circuit Plasticity? Neuroscientist. 2012; 18:28–44. [PubMed: 21551076]
10. Olmos-Serrano JL, et al. Defective GABAergic neurotransmission and pharmacological rescue of neuronal hyperexcitability in the amygdala in a mouse model of fragile X syndrome. J. Neurosci. 2010; 30:9929–9938. [PubMed: 20660275]
11. Curia G, Papouin T, Seguela P, Avoli M. Downregulation of tonic GABAergic inhibition in a mouse model of fragile X syndrome. Cereb. Cortex. 2009; 19:1515–1520. [PubMed: 18787232]
12. Gibson JR, Bartley AF, Hays SA, Huber KM. Imbalance of neocortical excitation and inhibition and altered UP states reflect network hyperexcitability in the mouse model of fragile X syndrome. J. Neurophysiol. 2008; 100:2615–2626. [PubMed: 18784272]
13. Testa-Silva G, et al. Hyperconnectivity and slow synapses during early development of medial prefrontal cortex in a mouse model for mental retardation and autism. Cereb. Cortex. 2012; 22:1333–1342. [PubMed: 21856714]
14. Miller LJ, et al. Electrodermal responses to sensory stimuli in individuals with fragile X syndrome: a preliminary report. Am. J. Med. Genet. 1999; 83:268–279. [PubMed: 10208160]
15. Golshani P, et al. Internally mediated developmental desynchronization of neocortical network activity. J. Neurosci. 2009; 29:10890–10899. [PubMed: 19726647]
16. Poulet JF, Petersen CC. Internal brain state regulates membrane potential synchrony in barrel cortex of behaving mice. Nature. 2008; 454:881–885. [PubMed: 18633351]
17. Grienberger C, Konnerth A. Imaging calcium in neurons. Neuron. 2012; 73:862–885. [PubMed: 22405199]
18. Rochefort NL, et al. Sparsification of neuronal activity in the visual cortex at eye-opening. Proc. Natl. Acad. Sci. U. S. A. 2009; 106:15049–15054. [PubMed: 19706480]
19. Cruz-Martin A, Crespo M, Portera-Cailliau C. Delayed stabilization of dendritic spines in fragile X mice. J. Neurosci. 2010; 30:7793–7803. [PubMed: 20534828]
20. Bureau I, Shepherd GM, Svoboda K. Circuit and plasticity defects in the developing somatosensory cortex of FMR1 knock-out mice. J Neurosci. 2008; 28:5178–5188. [PubMed: 18480274]
21. Harlow EG, et al. Critical period plasticity is disrupted in the barrel cortex of FMR1 knockout mice. Neuron. 2010; 65:385–398. [PubMed: 20159451]
22. Stern EA, Maravall M, Svoboda K. Rapid development and plasticity of layer 2/3 maps in rat barrel cortex in vivo. Neuron. 2001; 31:305–315. [PubMed: 11502260]
23. Cossart R, Aronov D, Yuste R. Attractor dynamics of network UP states in the neocortex. Nature. 2003; 423:283–288. [PubMed: 12748641]
24. Steriade M, Nunez A, Amzica F. A novel slow (< 1 Hz) oscillation of neocortical neurons in vivo: depolarizing and hyperpolarizing components. J. Neurosci. 1993; 13:3252–3265. [PubMed: 8340806]
25. Constantinople CM, Bruno RM. Effects and mechanisms of wakefulness on local cortical networks. Neuron. 2011; 69:1061–1068. [PubMed: 21435553]
26. Cowan RL, Wilson CJ. Spontaneous firing patterns and axonal projections of single corticostriatal neurons in the rat medial agranular cortex. J Neurophysiol. 1994; 71:17–32. [PubMed: 8158226]
27. Hays SA, Huber KM, Gibson JR. Altered Neocortical Rhythmic Activity States in Fmr1 KO Mice Are Due to Enhanced mGluR5 Signaling and Involve Changes in Excitatory Circuitry. J. Neurosci. 2011; 31:14223–14234. [PubMed: 21976507]

28. Li CY, Poo MM, Dan Y. Burst spiking of a single cortical neuron modifies global brain state. Science. 2009; 324:643–646. [PubMed: 19407203]
29. Veasey SC, et al. An automated system for recording and analysis of sleep in mice. Sleep. 2000; 23:1025–1040. [PubMed: 11145318]
30. Tanelian DL, Kosek P, Mody I, MacIver MB. The role of the GABAA receptor/chloride channel complex in anesthesia. Anesthesiology. 1993; 78:757–776. [PubMed: 8385426]
31. Franks NP, Lieb WR. Molecular and cellular mechanisms of general anaesthesia. Nature. 1994; 367:607–614. [PubMed: 7509043]
32. Pfeiffer BE, Huber KM. The state of synapses in fragile X syndrome. Neuroscientist. 2009; 15:549–567. [PubMed: 19325170]
33. Bassell GJ, Warren ST. Fragile X syndrome: loss of local mRNA regulation alters synaptic development and function. Neuron. 2008; 60:201–214. [PubMed: 18957214]
34. Olshausen BA, Field DJ. Sparse coding of sensory inputs. Curr. Opin. Neurobiol. 2004; 14:481–487. [PubMed: 15321069]
35. Musumeci SA, et al. Audiogenic seizures susceptibility in transgenic mice with fragile X syndrome. Epilepsia. 2000; 41:19–23. [PubMed: 10643918]
36. Van der Molen MJ, Van der Molen MW. Reduced alpha and exaggerated theta power during the resting-state EEG in fragile X syndrome. Biol. Psychol. 2013; 92:216–219. [PubMed: 23182872]
37. He C, Portera-Cailliau C. The trouble with spines in fragile X syndrome: density, maturity and plasticity. Neuroscience. 2012 E-pub ahead of print Apr 20.
38. D'Hulst C, Kooy RF. The GABAA receptor: a novel target for treatment of fragile X? Trends Neurosci. 2007; 30:425–431. [PubMed: 17590448]
39. LeBlanc JJ, Fagiolini M. Autism: a “critical period” disorder? Neural Plast. 2011; 2011:921680. [PubMed: 21826280]
40. Meredith RM, Dawitz J, Kramvis I. Sensitive time-windows for susceptibility in neurodevelopmental disorders. Trends Neurosci. 2012
41. Kronk R, et al. Prevalence, nature, and correlates of sleep problems among children with fragile X syndrome based on a large scale parent survey. Sleep. 2010; 33:679–687. [PubMed: 20469810]
42. Zhang J, et al. Fragile X-related proteins regulate mammalian circadian behavioral rhythms. Am. J. Hum. Genet. 2008; 83:43–52. [PubMed: 18589395]
43. Bushey D, Tononi G, Cirelli C. The Drosophila fragile X mental retardation gene regulates sleep need. J. Neurosci. 2009; 29:1948–1961. [PubMed: 19228950]
44. Castro-Alamancos MA. Cortical up and activated states: implications for sensory information processing. Neuroscientist. 2009; 15:625–634. [PubMed: 19321459]
45. Hagerman R, Hoem G, Hagerman P. Fragile X and autism: Intertwined at the molecular level leading to targeted treatments. Mol Autism. 2010; 1:12. [PubMed: 20858229]
46. Zhang L, He J, Jugloff DG, Eubanks JH. The MeCP2-null mouse hippocampus displays altered basal inhibitory rhythms and is prone to hyperexcitability. Hippocampus. 2008; 18:294–309. [PubMed: 18058824]
47. Markram K, Markram H. The intense world theory - a unifying theory of the neurobiology of autism. Front Hum Neurosci. 2010; 4:224. [PubMed: 21191475]
48. El Idrissi A, et al. Decreased GABA(A) receptor expression in the seizure-prone fragile X mouse. Neurosci. Lett. 2005; 377:141–146. [PubMed: 15755515]
49. Gentet LJ, et al. Unique functional properties of somatostatin-expressing GABAergic neurons in mouse barrel cortex. Nat. Neurosci. 2012; 15:607–612. [PubMed: 22366760]
50. Selby L, Zhang C, Sun QQ. Major defects in neocortical GABAergic inhibitory circuits in mice lacking the fragile X mental retardation protein. Neurosci. Lett. 2007; 412:227–232. [PubMed: 17197085]
51. Dutch-Belgian Fragile X Consortium. Fmr1 knockout mice: a model to study fragile X mental retardation. Cell. 1994; 78:23–33. [PubMed: 8033209]
52. Golshani P, Portera-Cailliau C. In vivo 2-photon calcium imaging in layer 2/3 of mice. J. Vis. Exp. 2008

53. Pologruto TA, Sabatini BL, Svoboda K. ScanImage: flexible software for operating laser scanning microscopes. Biomed. Eng. Online. 2003; 2:13. [PubMed: 12801419]

54. Guizar-Sicairos M, Thurman ST, Fienup JR. Efficient subpixel image registration algorithms. Opt. Lett. 2008; 33:156–158. [PubMed: 18197224]

55. Yaksi E, Friedrich RW. Reconstruction of firing rate changes across neuronal populations by temporally deconvolved Ca2+ imaging. Nat. Methods. 2006; 3:377–383. [PubMed: 16628208]

56. Mitra, P.; Bokil, H. Observed brain dynamics. Oxford University Press; New York: 2008.

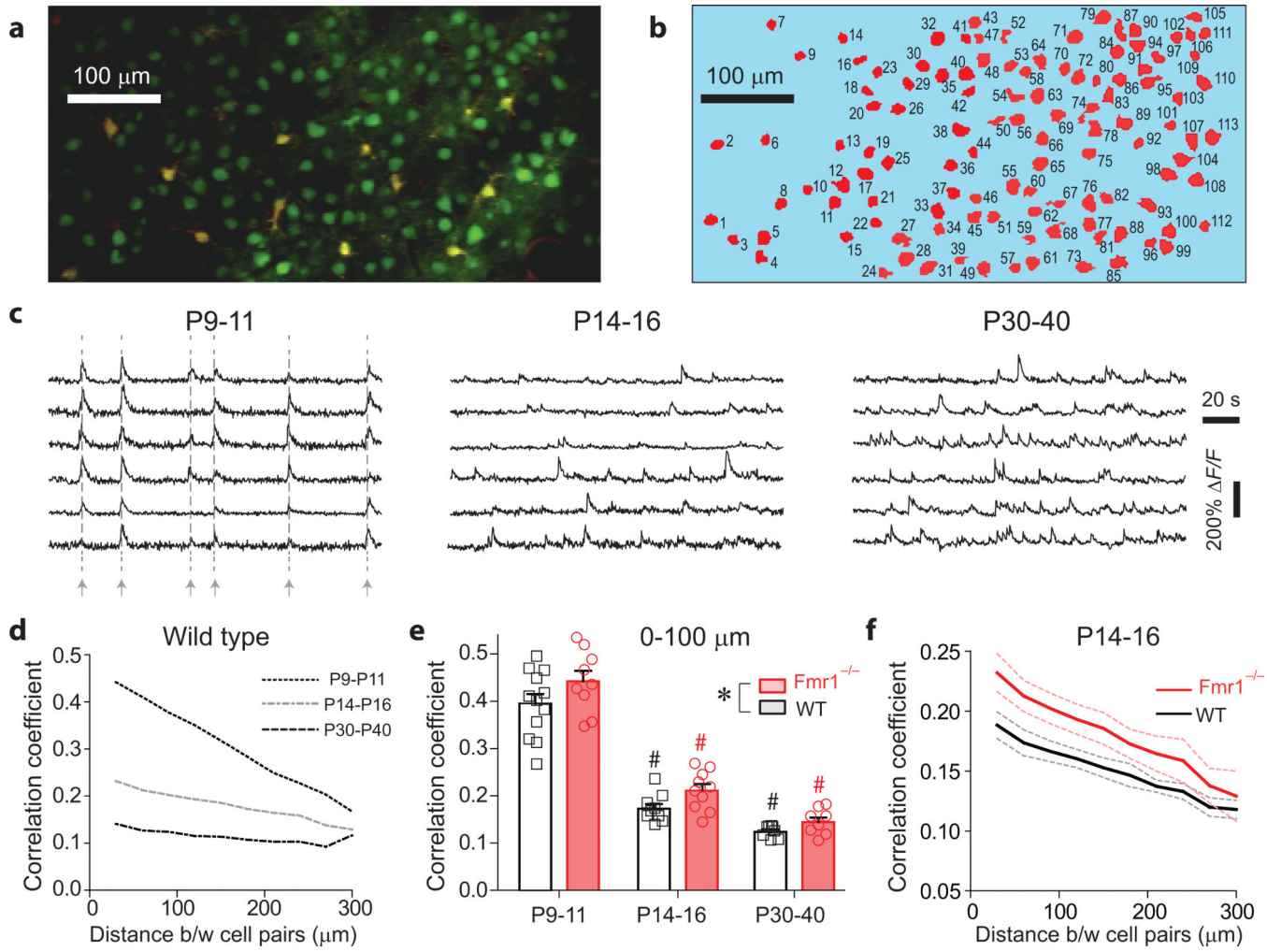

Figure 1. Delayed network desynchronization in the neocortex of unanesthetized *Fmr1*$^{-/-}$ mice

(a) Typical field of view of L2/3 neurons (green) stained with OGB-1 AM and imaged with in vivo two-photon microscopy. Sulforhodamine 101 was used to stain glia (yellow). Sum intensity projection (*xyt*) of a representative calcium imaging movie (3 min, 3.9 Hz) from a P15 mouse.

(b) Automated detection of neuronal cell bodies obtained through algorithmic segmentation of the image shown in *a*.

(c) Raw ΔF/F calcium traces of 6 different L2/3 neurons from representative movies at P9-11, P14-16 and P30-40. Gray arrows and vertical dashed lines represent times of synchronous firing.

(d) Mean correlation coefficients for all cell pairs vs. distance separating cell pairs in unanesthetized WT mice at different ages (n = 12, 9, 8 mice at P9-11, P14-16, and P30-40, respectively). The largest difference in correlation coefficients between P9-11 and P14-16 occurred for cell pairs <100 μm apart (Bonferroni corrected *p < 0.0001, two-way ANOVA).

(e) Mean correlation coefficients for all cell pairs within 100 μm of each other for WT (black) and *Fmr1*$^{-/-}$ (red) mice at different ages. For *Fmr1*$^{-/-}$ mice, n = 9, 10, 8 at P9-11,

P14-16, and P30-40, respectively. Both age and genotype significantly affected correlation coefficients (*$p < 0.05$ after Bonferroni correction, two-way ANOVA). The difference in correlation between WT and *Fmr1*$^{-/-}$ was largest at P14-16 (*$p = 0.039$, t-test). Error bars indicate the standard error of the mean (s.e.m.).

(f) Mean correlation coefficients vs. distance for WT and *Fmr1*$^{-/-}$ mice at P14-16. Dashed lines indicate s.e.m. boundaries.

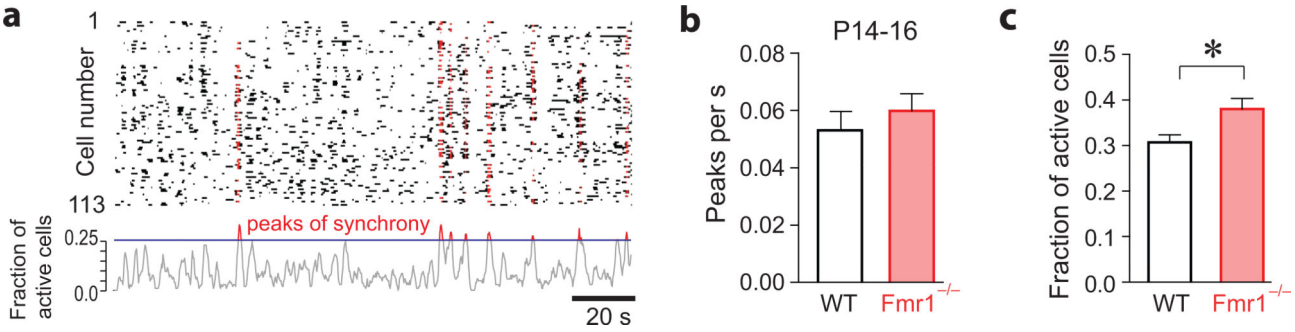

Figure 2. A higher proportion of L2/3 neurons are recruited to peaks of synchrony in unanesthetized *Fmr1*$^{-/-}$ mice

(a) Raster plot showing identified spiking events in L2/3 cells from a calcium movie in an unanesthetized WT mouse at P15 (same as Fig. 1a, b). Events shown in red were identified as having participated in a peak of synchrony (see Methods). The bottom trace shows the cumulative fraction of active cells over time.

(b) Mean frequency of peaks of synchrony in WT and *Fmr1*$^{-/-}$ mice at P14-16.

(c) Mean fraction of active L2/3 cells at the maximum point of each peak of synchrony in WT and *Fmr1*$^{-/-}$ mice at P14-16 (*p = 0.023, t-test).

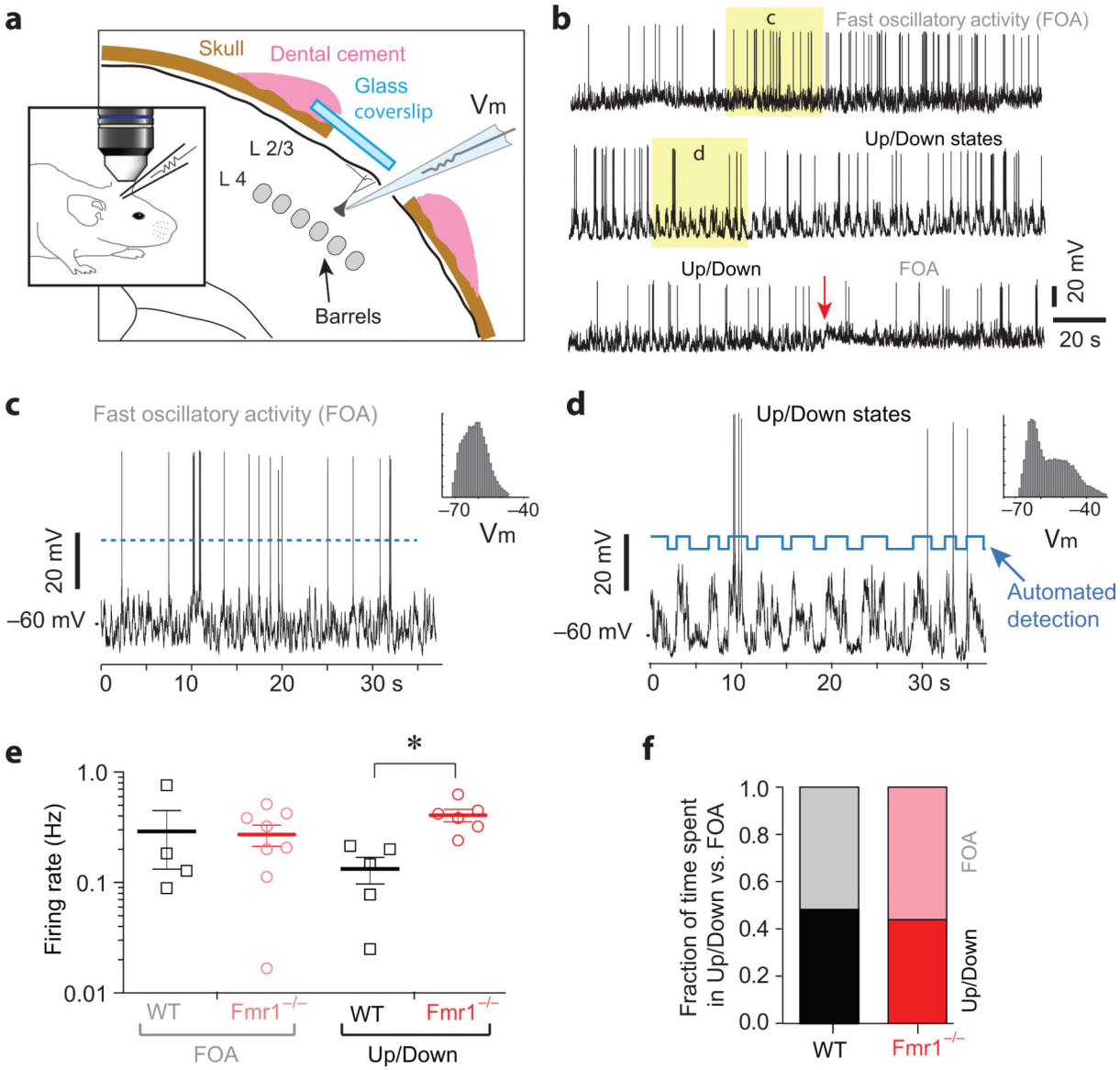

Figure 3. Elevated firing rates in unanesthetized *Fmr1*$^{-/-}$ mice during Up/Down states

(a) Cartoon of in vivo patch-clamp recordings of L2/3 neurons in barrel cortex of unanesthetized mice.

(b) Representative examples of whole-cell recordings (3 min long) in different behavioral brain states of the animal: Fast oscillatory activity (FOA; consistent with active wakefulness or REM sleep) and Up/Down states (consistent with slow-wave sleep or quiet wakefulness). The bottom trace shows a transition from Up & Down states to FOA. Note the movement artifact (arrow) when the animal transitions between the two different brain states. The segments highlighted in yellow are expanded in panels *c* and *d*.

(c, d) Traces with membrane potential (V_m) fluctuations typical of Up/Down states were algorithmically detected. Shown here are typical examples of FOA (e) and Up/Down state (f) recordings that were automatically sorted with this approach. Note that the latter exhibit a bimodal V_m distribution (insets).

(e) Firing rates for WT and *Fmr1*$^{-/-}$ mice during recordings in FOA vs. Up/Down brain states. *$p < 0.05$ after Bonferroni correction, 2-way ANOVA.
(f) Fraction of time spent in FOA vs. Up/Down states for WT and *Fmr1*$^{-/-}$ mice. There were no significant differences between genotypes.

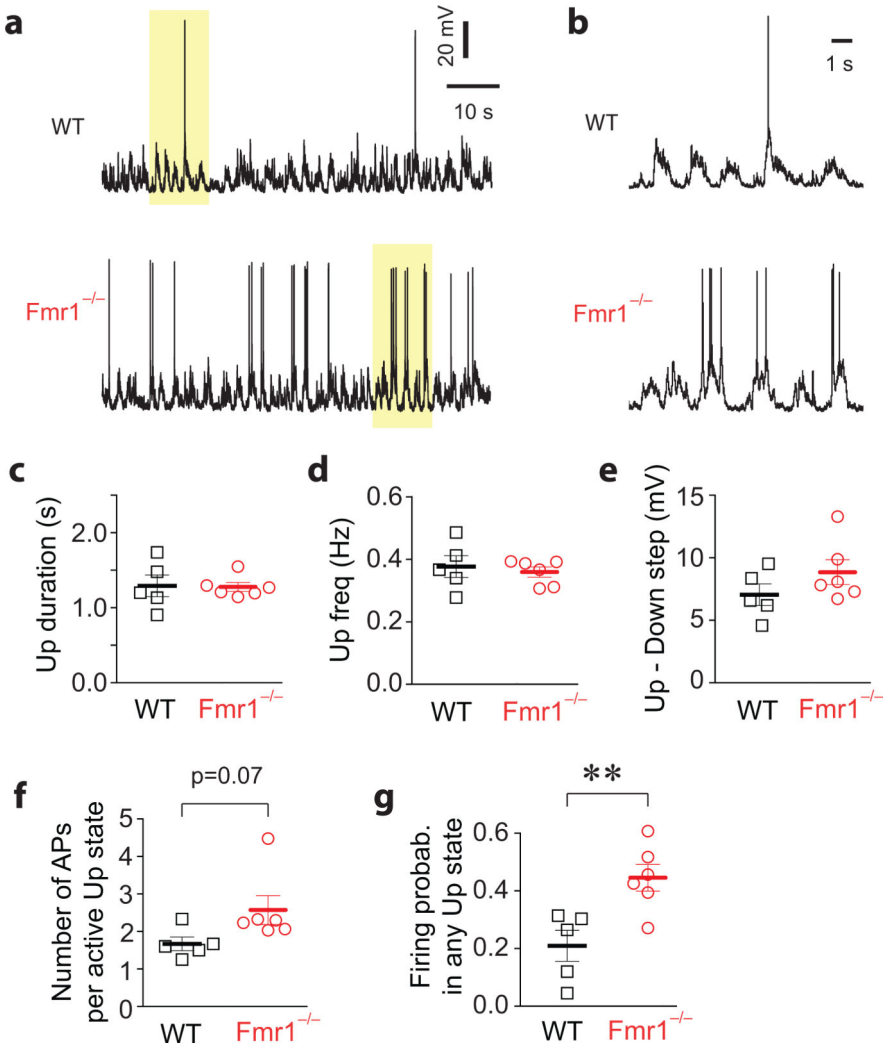

Figure 4. Higher probability of neuronal firing during Up states in *Fmr1*$^{-/-}$ mice

(a) Sample traces during Up/Down states from in vivo whole cell recordings of L2/3 neurons in unanesthetized WT (top) and *Fmr1*$^{-/-}$ mice (bottom). The highlighted segments are expanded in panel *b*.

(b) Expanded traces of Up & Down segments in WT (top) and *Fmr1*$^{-/-}$ mice (bottom).

(c, d) Mean duration (*c*) and frequency (*d*) of Up states in WT and *Fmr1*$^{-/-}$ mice. Note that not all recordings (or neurons) showed segments that were classified as Up/Down states (n = 5 and 6 recording segments with Up/Down states in WT and *Fmr1*$^{-/-}$ mice, respectively). There were no significant differences between genotypes.

(e) Mean Up-Down voltage step (in mV) in WT and *Fmr1*$^{-/-}$ mice. The trend toward higher step in mutant mice was not significant (p = 0.21, t-test).

(f) Mean number of action potentials per active Up state (i.e., Up states with 1 or more spikes) in WT and *Fmr1*$^{-/-}$ mice. p = 0.07, t-test.

(g) Mean firing probability during any given Up state (active or silent) in WT and *Fmr1*$^{-/-}$ mice. **p < 0.01, t-test.

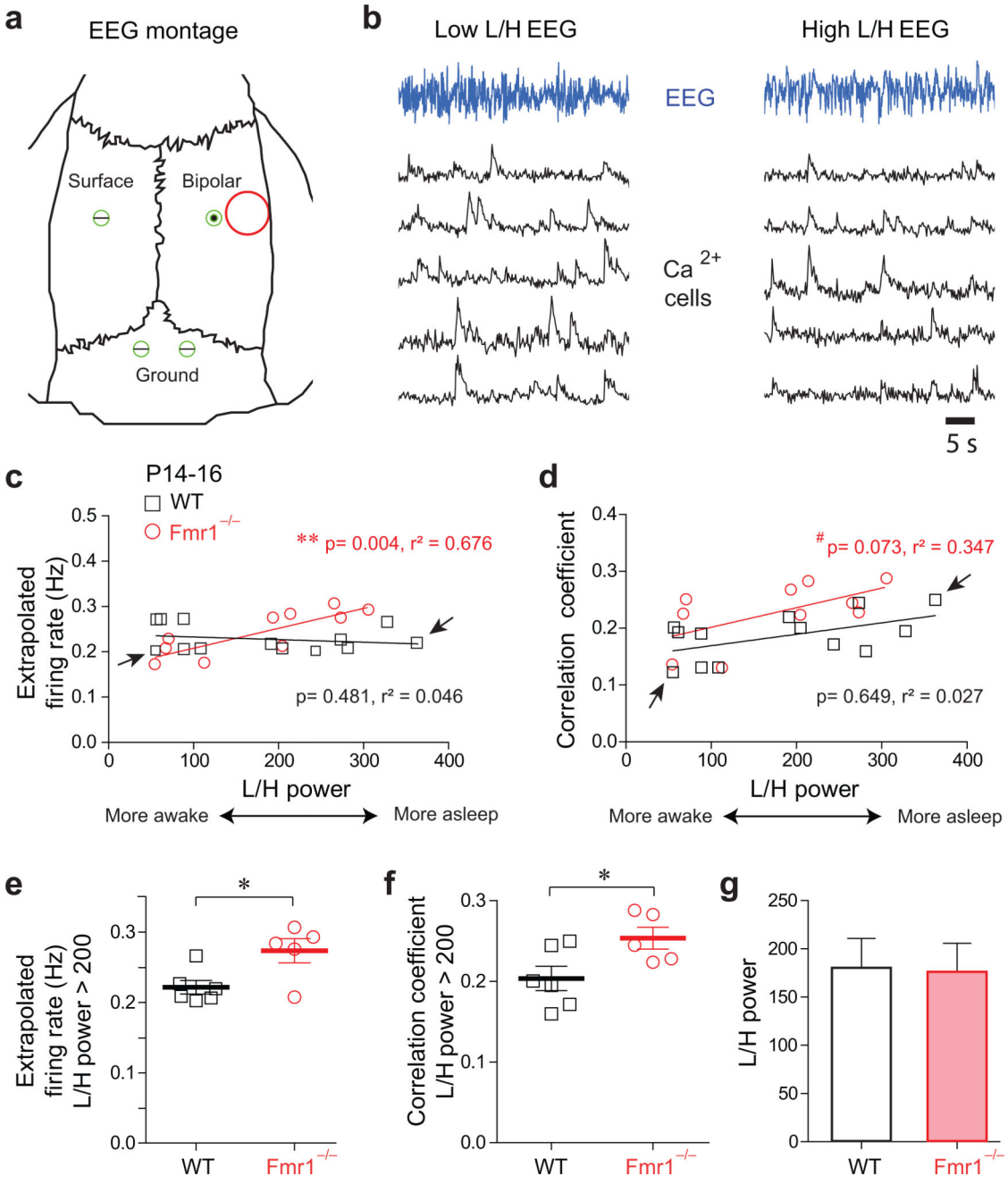

Figure 5. *Fmr1*$^{-/-}$ mice exhibit abnormal modulation of neuronal activity in different brain states

(a) Cartoon of the mouse skull showing the typical montage of EEG electrodes with respect to the cranial window (red circle) in the combined EEG and calcium imaging experiments. (b) Representative examples of calcium traces for individual cells during EEG recordings in unanesthetized WT mice at P14-16 manifesting low (left) or high(right) L/H power, which is a measure of the behavioral state of the animal[28]. Low and high L/H power is consistent with active wakefulness and sleep, respectively. Shown are typical calcium traces of 5 cells (black) and the EEG (blue; 20 Hz boxcar filter).

(c) Plot of mean estimated firing rates (extrapolated from calcium traces) and L/H power for WT and *Fmr1*$^{-/-}$ mice at P14-16. Each square and circle represents a different 3 min EEG/calcium imaging recording. Arrows point to the WT animals shown as examples in *b*. Lines represent linear-regression fits; statistics were done using an F-test.

(d) Plot of mean correlation coefficients and L/H power for WT and *Fmr1*$^{-/-}$ mice at P15-16.

(e, f) Mean estimated firing rates (e) and correlation coefficients (f) for EEG recordings with L/H power > 200 (which corresponds to sleep; Ref. 25). *p = 0.023 (d) and *p = 0.039 (f) (t-test).

(g) L/H power for WT and *Fmr1*$^{-/-}$ mice (p > 0.05, t-test).

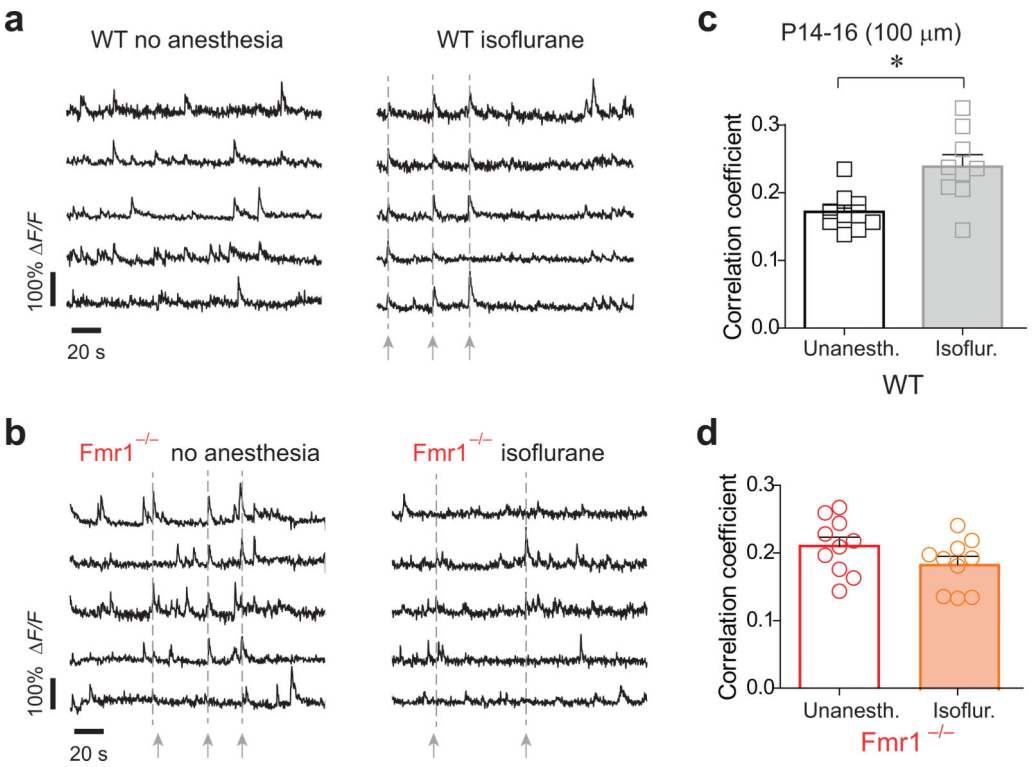

Figure 6. The synchrony of L2/3 cortical pyramidal neurons is not modulated by anesthesia in *Fmr1*$^{-/-}$ mice

(a, b) Typical examples of calcium traces for 5 cells in WT mice (a) and *Fmr1*$^{-/-}$ mice (b) during recordings at P14-16 without anesthesia (left) and under isoflurane anesthesia (right). The vertical dashed lines represent times of synchronous firing during recordings under anesthesia. Note also the higher synchrony of calcium transients in the *Fmr1*$^{-/-}$ mouse compared to the WT mouse.

(c, d) Mean correlation coefficients for all cell pairs (< 100 μm) in (*c*) WT mice (0.24 ± 0.02 vs. 0.17 ± 0.01, n = 9 and 9 mice, respectively; p = 0.0045, t-test) and (*d*) *Fmr1*$^{-/-}$ mice (0.21 ± 0.01 vs. 0.18 ± 0.01, n = 10 and 10 mice, respectively, p = 0.14, t-test), at P14-16. Calcium imaging was done under no anesthesia vs. with isoflurane anesthesia (1-2%, inh; n = 5 WT and 7 *Fmr1*$^{-/-}$ mice).